2012

Predicting shape and stability of air–water interface on superhydrophobic surfaces comprised of pores with arbitrary shapes and depths

B. Emami
Virginia Commonwealth University

Dr. Hooman Vahedi Tafreshi
Virginia Commonwealth University, htafreshi@vcu.edu

M. Gad-el-Hak
Virginia Commonwealth University, gadelhak@vcu.edu

Gary C. Tepper
Virginia Commonwealth University, gctepper@vcu.edu

Emami, B., Tafreshi, H.V., Gad-El-Hak, M., et al. Predicting shape and stability of air–water interface on superhydrophobic surfaces comprised of pores with arbitrary shapes and depths. Applied Physics Letters, 100, 013104 (2012).

Predicting shape and stability of air–water interface on superhydrophobic surfaces comprised of pores with arbitrary shapes and depths

B. Emami, H. Vahedi Tafreshi,[a] M. Gad-el-Hak, and G. C. Tepper
Department of Mechanical and Nuclear Engineering, Virginia Commonwealth University, Richmond, Virginia 23284-3015, USA

(Received 21 October 2011; accepted 9 December 2011; published online 4 January 2012)

An integro-differential equation for the three dimensional shape of air–water interface on superhydrophobic surfaces comprised of pores with arbitrary shapes and depths is developed and used to predict the static critical pressure under which such surfaces depart from the non-wetting state. Our equation balances the capillary forces with the pressure of the air entrapped in the pores and that of the water over the interface. Stability of shallow and deep circular, elliptical, and polygonal pores is compared with one another and a general conclusion is drawn for designing pore shapes for superhydrophobic surfaces with maximum stability. © *2012 American Institute of Physics*. [doi:10.1063/1.3673619]

A superhydrophobic surface can be made from a hydrophobic surface with micro or nanoroughness.[1,2] The superhydrophobicity effect is caused by a reduced solid–water contact area brought about by the air pockets entrapped in the porous structure of the rough surface when brought in contact with water. When the pore space on a superhydrophobic surface is filled with air, the system is said to be at the Cassie state.[3] Under elevated hydrostatic pressures, water can penetrate the pores and replace the air. The system then transitions to the so-called Wenzel state,[4] and the superhydrophobicity of the surface vanishes. The hydrostatic pressure at which a superhydrophobic surface departs from the Cassie state, whether or not it reaches the Wenzel state, is referred to as critical pressure.[5–7] Note that the focus of this study is the critical pressure of static or quasi-static penetration. Under dynamic penetration regimes, e.g., droplet impact on a superhydrophobic surface, the transition from Cassie state may occur at a much lower pressure.[8,9] Using balance of forces in a way similar to that used by[10–13] to study the meniscus stability on superhydrophobic surfaces with ordered microstructures, we recently calculated the shape and stability of the air–water interface on superhydrophobic surfaces comprised of randomly distributed posts of dissimilar sizes, heights, and materials.[14] In the formulations presented in Ref. 14, we assumed that the volume of the pore space is significantly larger than that of the displaced volume caused by the deflection of the air–water interface under pressure, and so the compression of the air entrapped in the pores was considered negligible. However, if the pores are shallow, compression of the air inside the pores can no longer be neglected. The first study to include the effects of the entrapped air compression in the force balance analysis is that of Salvadori *et al.*[15,16] These authors used balance of forces to predict the apparent contact angle of a droplet placed on superhydrophobic surfaces with circular or squared pores. The calculations reported in Refs. 15 and 16 are based on a simplifying assumption that regardless of the pore shape, the air–water meniscus inside a pore always maintains a constant curvature. That assumption is clearly suitable only for circular pores. In the present paper, we relax this restriction to better predict the actual shape of the air–water interface and to expand the force balance analysis to pores with arbitrary shapes.

Our formulations include balance of forces on the air–water interface of superhydrophobic surfaces with pores of arbitrary cross-sections, while accounting for the changes in the pressure of the entrapped air.

Our force balance analysis results in an integro-differential equation for the interface shape, which can be solved numerically to obtain the exact shape of the interface and the pressure at which the system departs from the Cassie state, i.e., the critical pressure. Such information is particularly consequential for designing microfabricated or disordered fibrous superhydrophobic coatings for underwater applications where resistance against elevated hydrostatic pressure is crucially important.[17–27]

It is worth noting that the Cassie and Wenzel states of a superhydrophobic surface have also been studied from a surface thermodynamics viewpoint. For example, Marmur[28] used minimization of surface energies to determine the apparent contact angles of a droplet on a superhydrophobic surface at Cassie and Wenzel states, where the air–water menisci on the surface were assumed to remain flat. Tuteja *et al.*[29] extended this method to calculate the corresponding critical pressure. As they pointed out, this yields a critical pressure which is not even in a qualitative agreement with experiment. They argued that this is because of the flat air–-water interface assumption.

In the current study, we apply our analysis to various simple geometries, namely circular, elliptical, and polygonal pores. These primitive geometries are in fact the building blocks of more complicated ordered/disordered microstructures that can be manufactured with different techniques (or found in nature). Fig. 1 shows examples of superhydrophobic surfaces comprised of holes of different shapes, one manufactured by anodization of aluminum in oxalic and sulfuric acids[27] and the other via electrospinning[22] (also see Refs. 8 and 9).

[a]Author to whom correspondence should be addressed. Electronic mail: htafreshi@vcu.edu. Tel.: 804-828-9936. Fax: 804-827-7030.

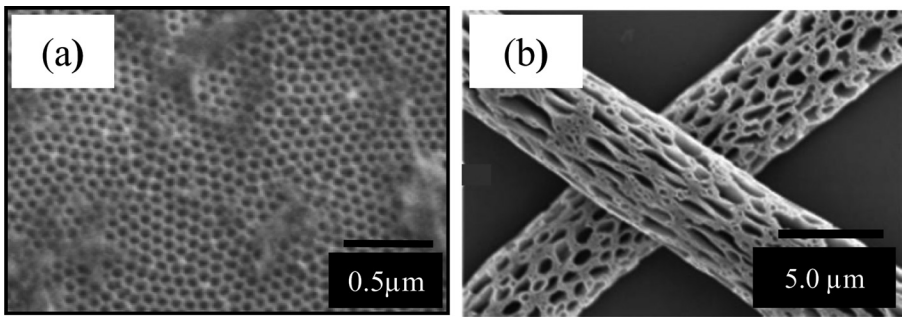

FIG. 1. Examples of superhydrophobic surfaces comprised of individual pores: (a) surface made of anodic alumina film coated with a hydrophobic polymer.[27] (b) Electrospun polystyrene fiber.[22]

Fig. 2 is a sketch of the air–water meniscus corresponding to a circular pore in an axisymmetric coordinate system (given the axisymmetry, only half of the interface is shown). Applying balance of forces and using the Young–Laplace law, one obtains

$$P + P_\infty - P_a - \sigma \nabla \cdot \vec{n} = 0 \tag{1}$$

where P, P_∞, and P_a are, respectively, the hydrostatic, atmospheric, and entrapped air pressures, σ is the surface tension, and $\vec{n}$ is the interface unit normal vector. Let $y = g(r)$ be the surface shape, where r and y are the radial and axial coordinates, respectively. It can be shown that $n_r = g'(1+g'^2)^{-1/2}$ and $n_y = -(1+g'^2)^{-1/2}$, where $'$ represents derivative with respect to r, and n_r and n_y are the components of $\vec{n}$ in the r and y directions, respectively. The shape of the air–water interface changes with the hydrostatic pressure P. This consequently changes the volume, and therefore, the pressure of the air entrapped in the pore, P_a. Here, we assume that dissolution of the entrapped air into water is insignificant, and therefore the air does not escape from the pores when the surface is in Cassie state. Because the entrapped air is in a thermal equilibrium with the water, one could assume an isothermal equilibrium. The ideal gas law thus yields $P_a = P_\infty V_{a,0}/V_a$, where $V_{a,0}$ is the pore volume (volume of the entrapped air at $P = 0$), and V_a is the entrapped air volume.

It can be shown that $V_a = V_{a,0} + 2\pi \int_0^{w_c/2} rg(r)dr$, where w_c is the diameter of the circular pore. Equation (1) then reduces to

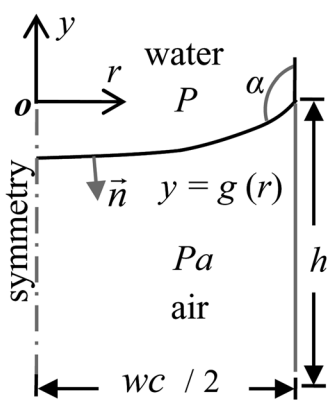

FIG. 2. Force balance diagram in an axisymmetric coordinate system corresponding to the air–water interface over a circular pore.

$$\frac{\sigma}{r}(rg'' + g' + g'^3) - \left[P + P_\infty\left(1 - \frac{V_{a,0}}{V_{a,0} + 2\pi\int_0^{w_c/2} rg(r)dr}\right)\right](1+g'^2)^{3/2} = 0 \tag{2}$$

subject to $g'(0) = 0$ and $g(w_c/2) = 0$, where r represents the radial coordinate, $g(r)$ describes the shape of the interface, and $V_{a,0}$ is the pore volume. The above integro-differential equation can be solved numerically to calculate the shape of the interface at different hydrostatic pressures. At the critical hydrostatic pressure, the angle between the interface and the solid wall (angle α in Fig. 2(a)) reaches θ, the water–air–solid equilibrium contact angle.[7,10–14] In this case, because of the balance between the pressure and capillary forces, $-\sigma\cos\theta = (P + P_\infty - P_a)w_c/4$. Equation (2) then becomes

$$\frac{\sigma}{r}(g''_{cr} + g'_{cr} + g'^3_{cr})(1+g'^2_{cr})^{-3/2} + \frac{4\cos\theta}{w_c} = 0, \tag{3}$$

where $g_{cr}(r)$ is the interface shape at the critical pressure. The critical pressure is then calculated as

$$P_{cr} = P_\infty\left(\frac{V_{a,0}}{V_{a,0} + 2\pi\int_0^w g_{cr}(x)dx} - 1\right) - \frac{\sigma\cos\theta}{w_c}. \tag{4}$$

A similar approach is used to derive a more general equation in a Cartesian coordinate system for the interface of a superhydrophobic surface with pores of arbitrary cross-sections. Applying balance of forces, and assuming $z = F(x,y)$ is the interface shape, one gets

$$(1+F_y^2)F_{xx} + (1+F_x^2)F_{yy} - 2F_xF_yF_{xy} - \left[P + P_\infty\left(1 - \frac{V_{a,0}}{V_{a,0} + \int_0^w\int_0^w F(x,y)dxdy}\right)\right](1+F_x^2+F_y^2)^{3/2} = 0, \tag{5}$$

where the subscripts x and y represent $\partial/\partial x$ and $\partial/\partial y$, respectively.

As per the boundary conditions, F vanishes on the walls. Similar to the previous cases, the surface departs from the Cassie state, and hence superhydrophobicity vanishes, if the angle between the interface and the solid wall (on the liquid side) exceeds the equilibrium contact angle, θ. Therefore, the surface remains superhydrophobic if $|\nabla F| < |\cot\theta|$. The critical pressure can then be calculated by solving Eq. (5) at

various hydrostatic pressures. The pressure at which the maximum $|\nabla F|$ equals $|\cot\theta|$ is the critical pressure. Obviously, either of Eqs. (4) or (5) can be used to calculate the critical pressure of a circular pore. Equation (4), although restricted to circular pores, is advantageous over Eq. (5), because it is deterministic.

We used the FlexPDE program from PDE Solutions, Inc., to solve Eqs. (3) and (5) via the finite element method. The calculations were performed on a workstation with a dual core 2.4 GHz processor and 4 GB of memory. Each solution took only a few seconds. Careful attention was paid to ensure that the results of our calculations are not dependent on the choice of the mesh size. For all the geometries discussed in this paper, we considered $h = 2.5\ \mu$m and $\theta = 120°$. For the ease of comparison, we used a diameter w_c of $10\ \mu$m for the circular pores. The dimensions of the other geometries (polygons and ellipses) were then calculated assuming that the cross-sectional areas were identical.

We used our method to calculate the critical pressure for a circular pore as well as a wide range of elliptical and polygonal pores. Fig. 3(a) shows the air–water interface F and the $|\nabla F|$ contours for a circular pore at its critical pressure of 52 kPa. Note that discounting the pressure rise inside the pore (i.e., setting the integral terms in Eq. (5) equal to zero), results in an under-predicted critical pressure of 14.3 kPa. It is worth mentioning that solving Eq. (3) (axisymmetric coordinate system) for the circular pore yields identical results, as expected. Some of the results for the elliptical and polygonal pores are shown in Figs. 3(b)–3(d), presenting the air–water interfaces and the gradient contours at the corresponding critical pressures. For each case, the critical pressure was calculated by solving Eq. (5) at different hydrostatic pressures, until $|\nabla F| < \cot\theta = 0.58$ is violated at any point on the wall boundaries. Note that blue to red in the contours corresponds to 0–0.6.

Fig. 4(a) shows the calculated critical pressures for the polygonal pores, ranging from an equilateral triangle ($n = 3$) to an equilateral polygon with 100 sides. The pressure is normalized by the critical pressure of the circular pore, $P_{cr}^{\infty} = 52$ kPa. Fig. 4(b) presents similar results produced for the elliptical pores, with a minor-to-major diameter ratio η ranging from 0.3 to 1. Note that a circular shape is a special case of the polygonal and elliptical cross-sections when $n \to \infty$ and $\eta = 1$, respectively. As can be seen, the critical pressure increases with n and η for, respectively, the polygonal and elliptical pores.

The insets of Figs. 4(a) and 4(b) show the critical pressures calculated when neglecting the pressure rise in the entrapped air. Again, the critical pressure values are normalized by that of the circular pore $P_{cr}^{\infty} = 14.3$ kPa. Note that calculations performed neglecting the pressure rise in the entrapped air significantly under-estimate the critical pressure. Also note that the relationship between the pore shape

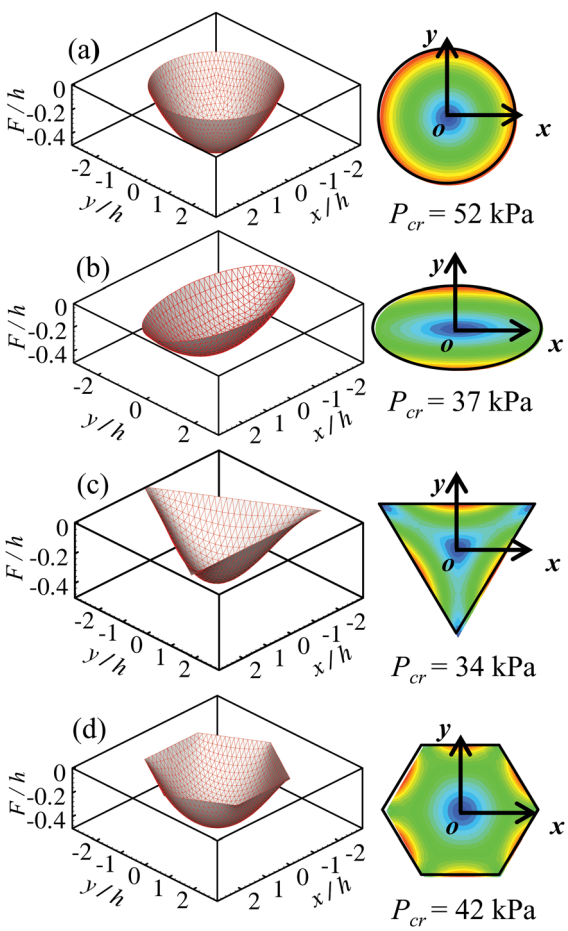

FIG. 3. (Color online) Calculated air–water interface at the critical hydrostatic pressures, over pores with (a) circular, (b) elliptical, (c) triangular, and (d) hexagonal cross-sections. Contour plots show the interface gradient value, $|\nabla F|$. Contour values correspond to 0–0.6. The critical pressure is determined based on the value of $|\nabla F|$.

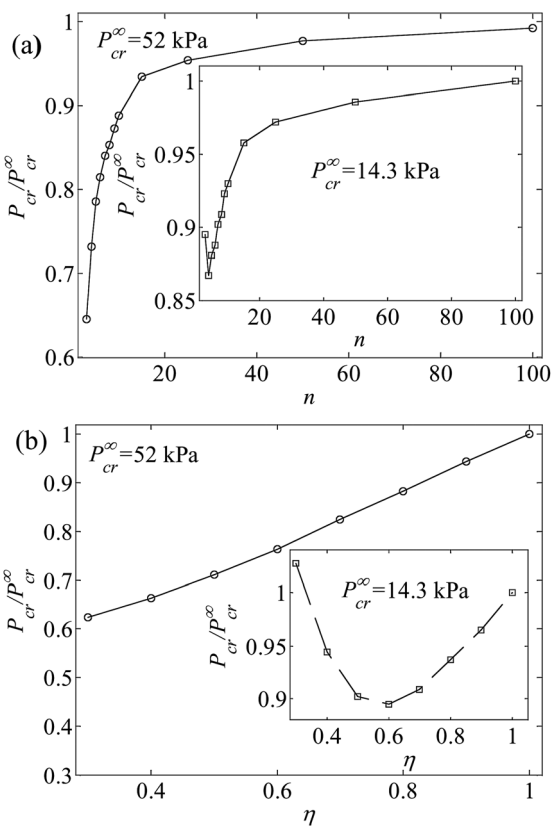

FIG. 4. Normalized critical pressure for a wide range of (a) polygonal and (b) elliptical pores all having identical cross-sectional areas.

and critical pressure is different when the effect of air compression is not considered, as can be seen clearly from the inset figures. The minimum critical pressure corresponds to $n = 4$ (squared pores) and $\eta = 0.6$ for the polygonal and elliptical pores. This is because in the absence of air compression effects, the critical pressure only depends on the balance between the capillary and hydrostatic forces. As the pore shape becomes more circular (i.e., as n and η increase), its perimeter decreases (note that all pores have identical cross-sectional areas). Obviously, the critical pressure should decrease with perimeter, because of the reduced capillary forces. On the other hand, as n and η increase, the pore shape, and hence the meniscus slope on the pore walls, becomes more uniform over the perimeter. As the meniscus instability depends on the local slope of the meniscus, the pore resistance to hydrostatic pressure increases when its shape becomes more circular. The critical pressure hence depends primarily on the balance between the effects of perimeter and homogeneity of the local slope of the meniscus. However, when the pressure rise in the entrapped air is included in the calculations, the effect of perimeter becomes less significant, and therefore the critical pressure mostly depends on the homogeneity of the meniscus slope near the pore walls. This is because the compression forces produced by the entrapped air are much higher than the capillary forces on the perimeter.

The authors would like to acknowledge the financial support for this work provided Defense Advanced Research Projects Agency (DARPA) Contract No. W91CRB-10-1-0003. In addition, BE and HVT also acknowledge VCU Presidential Research Incentive Program (PRIP) for partial support. The authors acknowledge Professor Bandyopadhyay of VCU School of Engineering for Fig. 1(a).

[1]J. Wang, F. Liu, H. Chen, and D. Chen, Appl. Phys. Lett. **95**, 084104 (2009).
[2]J. P. Rothstein, Annu. Rev. Fluid Mech. **42**, 89 (2010).
[3]A. B. D. Cassie and S. Baxter, Trans. Faraday Soc. **40**, 546 (1944).
[4]R. N. Wenzel, Ind. Eng. Chem. **28**, 988 (1936).
[5]B. Liu and F. F. Lange, J. Colloid Interface Sci. **298**, 899 (2006).
[6]X. Sheng and J. Zhang, Colloids Surf., A **377**, 374 (2011).
[7]B. Emami, T. M. Bucher, H. V. Tafreshi, M. Gad-el-Hak, and G. C. Tepper, Colloids Surf., A **385**, 95 (2011).
[8]A. N. Lembach, H. -B. Tan, I. V. Roisman, T. Gambaryan-Roisman, Y. Zhang, C. Tropea, and A. L. Yarin, Langmuir **26**, 9516 (2010).
[9]C. M. Weickgenannt, Y. Zhang, A. N. Lembach, H -B. Tan, I. V. Roisman, T. Gambaryan-Roisman, A. L. Yarin, and C. Tropea, Phys. Rev. E **83**, 036305 (2011).
[10]C. W. Extrand, Langmuir **18**, 7991 (2002).
[11]C. W. Extrand, Langmuir **20**, 5013 (2004).
[12]Q. S. Zheng, Y. Yu, and Z. H. Zhao, Langmuir **21**, 12207 (2005).
[13]E. J. Lobaton and T. R. Salamon, J. Colloid Interface. Sci. **314**, 184 (2007).
[14]B. Emami, H. V. Tafreshi, M. Gad-el-Hak, and G. C. Tepper, Appl. Phys. Lett. **98**, 203106-1 (2011).
[15]M. C. Salvadori, M. Cattani, M. R. S. Oliveira, F. S. Teixeira, and I. G. Brown, Appl. Phys. Lett. **96**, 074101 (2010).
[16]M. C. Salvadori, M. Cattani, M. R. S. Oliveira, F. S. Teixeira, and I. G. Brown, J. Appl. Phys. **108**, 024908 (2010).
[17]A. Marmur, Langmuir **22**, 1400 (2006).
[18]M. Sakai, T. Yanagisawa, A. Nakajima, Y. Kameshima, and K. Okada, Langmuir **25**, 13 (2009).
[19]M. S. Bobji, S. V. Kumar, A. Asthana, and R. N. Govardhan, Langmuir **25**(20), 12120 (2009).
[20]R. Poetes, K. Holtzmann, K. Franze, and U. Steiner, Phys. Rev. Lett., **105**, 166104 (2010).
[21]M. A. Samaha, F. O. Ochanda, H. V. Tafreshi, G. C. Tepper, and M. Gad-el-Hak, Rev. Sci. Instrum. **82**, 045109-1 (2011).
[22]O. Ochanda, M. A. Samaha, H. V. Tafreshi, G. C. Tepper, and M. Gad-el-Hak, J. Appl. Polym. Sci. **123**, 1112 (2011).
[23]P. Forsberg, F. Nikolajeff, and M. Karlsson, Soft Matter **7**, 104 (2011).
[24]C. Lee and C. J. Kim, Phys. Rev. Lett. **106**, 014502 (2011).
[25]G. Whyman and E. Bormashenko, Langmuir **27**, 8171 (2011).
[26]B. Emami, H. V. Tafreshi, M. Gad-el-Hak, and G. C. Tepper, "Effect of Fiber Orientation on Shape and Stability of Air–Water Interface on Submerged Superhydrophobic Electrospun Thin Coatings," J. Appl. Phys. (submitted).
[27]J. N. Mateo, S. S. Kulkarni, L. Das, S. Bandyopadhyay, G. C. Tepper, K. J. Wynne, and S. Bandyopadhyay, Nanotechnology **22**, 1 (2011).
[28]A. Marmur, Langmuir **19**, 8343 (2003).
[29]A. Tuteja, W. Choi, J. M. Mabry, G. H. McKinely, and R. E. Cohen, Proc. Natl. Acad. Sci. U.S.A. **105**, 18200 (2008).